Journal of Solid State Chemistry 206 (2013) 20–26

Contents lists available at ScienceDirect

Journal of Solid State Chemistry

journal homepage: www.elsevier.com/locate/jssc

A high-pressure route to thermoelectrics with low thermal conductivity: The solid solution series $AgIn_xSb_{1-x}Te_2$ ($x=0.1$–0.6)

Thorsten Schröder [a], Tobias Rosenthal [a], Daniel Souchay [a], Christian Petermayer [a], Sebastian Grott [a], Ernst-Wilhelm Scheidt [b], Christian Gold [b], Wolfgang Scherer [b], Oliver Oeckler [c,*]

[a] LMU Munich, Department of Chemistry, Butenandtstraße 5-13 (D), 81377 Munich, Germany
[b] University of Augsburg, Institut für Physik, Universitätsstraße 1, 86159 Augsburg, Germany
[c] Leipzig University, IMKM, Scharnhorststraße 20, 04275 Leipzig, Germany

ARTICLE INFO

Article history:
Received 7 June 2013
Received in revised form
18 July 2013
Accepted 21 July 2013
Available online 29 July 2013

Keywords:
Silver indium antimony telluride
Thermoelectric properties
High-pressure synthesis
Electron microscopy
Phase transitions
Solid solutions

ABSTRACT

Metastable rocksalt-type phases of the solid solution series $AgIn_xSb_{1-x}Te_2$ ($x=0.1$, 0.2, 0.4, 0.5 and 0.6) were prepared by high-pressure synthesis at 2.5 GPa and 400 °C. In these structures, the coordination number of In^{3+} is six, in contrast to chalcopyrite ambient-pressure $AgInTe_2$ with fourfold In^{3+} coordination. Transmission electron microscopy shows that real-structure phenomena and a certain degree of short-range order are present, yet not very pronounced. All three cations are statistically disordered. The high degree of disorder is probably the reason why $AgIn_xSb_{1-x}Te_2$ samples with $0.4<x<0.6$ exhibit very low thermal conductivities with a total $\kappa<0.5$ W/K m and a lattice contribution of κ_{ph} ~0.3 W/K m at room temperature. These are lower than those of other rocksalt-type tellurides at room temperature; e.g. the well-known thermoelectric $AgSbTe_2$ (κ ~0.6 W/K m). The highest ZT value (0.15 at 300 K) is observed for $AgIn_{0.5}Sb_{0.5}Te_2$, mainly due to its high Seebeck coefficient of 160 μV/K. Temperature-dependent X-ray powder patterns indicate that the solid solutions are metastable at ambient pressure. At 150 °C, the quaternary compounds decompose into chalcopyrite-type $AgInTe_2$ and rocksalt-type $AgSbTe_2$.

1. Introduction

The interconversion of thermal and electrical energy by means of thermoelectrics is intensely researched, the long-term goal being the efficient generation of electrical energy from waste heat and the development of novel materials for Peltier coolers or small heating devices. The dimensionless figure of merit $ZT=S^2\sigma T/\kappa$ (Seebeck coefficient S, electrical conductivity σ, thermal conductivity κ) [1] is a measure of the efficiency of the conversion process. All quantities involved depend on the charge carriers' concentration and mobility and therefore cannot be optimized independently. According to the Wiedemann–Franz law, σ and the electronic part of the thermal conductivity (κ_{el}) are proportional to each other. Increasing the mobility of the charge carriers and thus σ, in addition, usually lowers the absolute value of S.

Therefore, a common approach to improving thermoelectrics aims at decreasing the phononic part of the thermal conductivity (κ_{ph}) without significantly interfering with the electronic properties. This paradigm suggests that effective phonon scattering is important, which can be achieved by creating nano-domain structures, e.g. twin domains in TAGS, i.e. $(AgSbTe_2)_{1-n}(GeTe)_n$ [2–4], or short-range ordered defect layers in GST materials, i.e. $(GeTe)_nSb_2Te_3$ [5,6]. Domain structures often result from phase transitions or, in case of heterogeneous systems, from partial phase separation [7–14]. Exsolution may lead to endotactic nanodots, e.g. in LAST ($AgPb_nSbTe_{2+n}$) [15]. As nanostructures and other real-structure effects as well as phase transitions play an important role, transmission electron microscopy and temperature-dependent X-ray diffraction are very valuable tools for structure elucidation.

Synthetic approaches to lowering κ_{ph} may include the application of high pressure or fast quenching (e.g. melt spinning) during crystallization. Stress as well as short crystallization times usually yield smaller grain sizes (i.e. more grain boundaries) and more pronounced real-structure effects. Both features may scatter phonons more effectively than electrons [16,17].

A large number of ternary I–V–VI_2 phases exhibit very low intrinsic thermal conductivities (<1 W/K m) [18,19], the most prominent compound being $AgSbTe_2$ with $k\approx0.6$ W/K m at room temperature (RT). It is characterized by ZT values of ~0.3 at RT and

* Correspondence to: Institute for Mineralogy, Crystallography and Materials Science, Leipzig University, Scharnhorststraße 20, 04275 Leipzig, Germany. Fax: +49 341 97 36299.
E-mail address: oliver.oeckler@gmx.de (O. Oeckler).

0022-4596/$ - see front matter © 2013 Elsevier Inc. All rights reserved.
http://dx.doi.org/10.1016/j.jssc.2013.07.027

Table 1
EDX results for $AgIn_xSb_{1-x}Te_2$ (averaged from 5 point analyses each).

Sum formula	Atom-% (calc.)	Atom-% (EDX)
$AgIn_{0.6}Sb_{0.4}Te_2$	Ag: 25; In: 15; Sb: 10; Te: 50	Ag: 23.1(7); In: 14.8(4); Sb: 11.6(3); Te: 50.5(9)
$AgIn_{0.5}Sb_{0.5}Te_2$	Ag: 25; In: 12.5; Sb: 12.5; Te: 50	Ag: 24.2(3); In: 12.1(6); Sb: 13.5(5); Te: 50.2(5)
$AgIn_{0.4}Sb_{0.6}Te_2$	Ag: 25; In: 10; Sb: 15; Te: 50	Ag: 24.9(5); In: 8.9(3); Sb: 16.0(5); Te: 50.2(6)
$AgIn_{0.2}Sb_{0.8}Te_2$	Ag: 25; In: 5; Sb: 20; Te: 50	Ag: 24.5(4); In: 4.5(3); Sb: 20.9(3); Te: 50.1(4)
$AgIn_{0.1}Sb_{0.9}Te_2$	Ag: 25; In: 2.5; Sb: 22.5; Te: 50	Ag: 24.5(5); In: 2.2(5); Sb: 23.5(5); Te: 49.7(6)

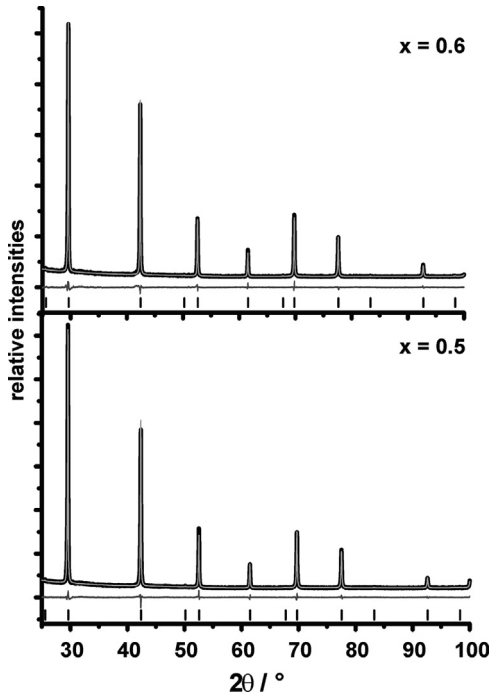

Fig. 1. Rietveld fits for $AgIn_{0.5}Sb_{0.5}Te_2$ (bottom) and $AgIn_{0.6}Sb_{0.4}Te_2$ (top); experimental (black) and calculated data (gray); difference plot (gray, below), peak positions (black, vertical lines).

up to 1.3 at 400 °C, respectively [20]; and represents both the end member of TAGS solid solutions and the matrix of LAST materials [2–4,15]. All of these materials, including nanostructured ones, exhibit cation disorder in sometimes distorted rocksalt-type crystal structures.

In contrast to $AgSbTe_2$, $AgInTe_2$ crystallizes in the chalcopyrite structure type, a superstructure of the sphalerite type where all cations are tetrahedrally coordinated by Te. In accordance with the pressure-coordination rule, $AgInTe_2$ transforms to a rocksalt-type structure under high pressure; however, phases with tetrahedrally coordinated In^{3+} are formed again after decompression within a few days [21]. For $AgInSe_2$, rocksalt-type high-pressure phases are metastable at ambient pressure when In is partially substituted by Sb [22]. Thus, one can expect that cation-disordered rocksalt-type members of a solid solution series $AgInTe_2$–$AgSbTe_2$ are accessible by high-pressure high-temperature syntheses and may be metastable at ambient conditions. For these phases, no thermoelectric data are available. However, chalcopyrite-type $AgInTe_2$ exhibits a thermal conductivity of ~2 W/K m at 300 K [14,23], more than three times higher than that of $AgSbTe_2$. The thermal conductivities of quaternary solid solutions may be expected to be even lower than those of ternary I–V–VI_2 compounds due to the fact that the number of disordered cation types is higher.

The element combination Ag/In/Sb/Te ("AIST") is an intriguing one as it plays an important role in the field of phase-change materials for rewritable optical data storage (e.g. $Ag_{3.4}In_{3.7}Sb_{76.4}Te_{16.5}$ on CD-RWs) [24]. As the required material properties for phase-change materials are comparable to those for thermoelectrics [5], the present study aims at characterizing the thermoelectric properties and structural features as well as stability ranges of AIST materials prepared by high-pressure high-temperature synthesis.

2. Experimental

2.1. Synthesis

Bulk samples with the nominal compositions $AgIn_xSb_{1-x}Te_2$ (x=0.1, 0.2, 0.4, 0.5 and 0.6) were prepared by heating stoichiometric mixtures (e.g., 1.5 g) of the pure elements (silver 99.9999%, Alfa Aesar; indium 99.999%, Smart Elements; antimony 99.9999%, Smart Elements; tellurium 99.999%, Alfa Aesar) in sealed silica glass ampoules to 950 °C under argon atmosphere. The resulting melts were quenched to RT in water. They contain mixtures of chalcopyrite-type $AgInTe_2$ and rocksalt-type $AgSbTe_2$ and were used as starting materials for high-pressure syntheses.

High-pressure experiments were performed using a multi-anvil hydraulic press (Voggenreiter, Mainleus, Germany) [25–28]. Quenched $AgIn_xSb_{1-x}Te_2$ was powdered, loaded into a cylindrical crucible made of hexagonal BN (Henze, Kempten, Germany) and sealed with a BN cap. In order to obtain an electrical resistance furnace; the capsule was centered within two nested graphite tubes. The remaining volume at both ends of the outer graphite tube was filled with two MgO discs. The arrangement, surrounded by a zirconia tube, was then placed into a pierced truncated Cr_2O_3-doped MgO octahedron (edge length 25 mm, Ceramic Substrates & Components, Isle of Wight, Great Britain). Eight truncated tungsten carbide cubes (truncation edge length 17 mm) served as anvils for the compression of the truncated octahedron, they were separated by pyrophyllite gaskets. The graphite tubes were electrically contacted by two Mo plates. The assembly was compressed up to a pressure of 2.5 GPa in 2 h. At this constant pressure, samples were prepared by annealing at 400 °C for 5 h and subsequently quenching the sample by turning off the furnace. After quenching the sample, the pressure was maintained for 1 h to ensure that RT was reached. Subsequently, the pressure was reduced to ambient pressure within 6 h.

2.2. EDX analysis

EDX (energy dispersive X-Ray) spectra of representative pieces of crushed bulk samples were recorded using a JSM-6500F (Jeol, USA) scanning electron microscope with EDX detector (model 7418, Oxford Instruments, Great Britain). For each sample, the results of five point analyses were averaged and the errors were estimated from their variance (see Table 1).

2.3. X-ray diffraction

X-ray powder patterns were recorded with a Huber G670 Guinier camera equipped with a fixed imaging plate and integrated read-out